

Barrier-free subsurface incorporation of 3d metal atoms into Bi(111) filmsC. Klein,^{1,*} N. J. Vollmers,² U. Gerstmann,^{2,†} P. Zahl,³ D. Lükermann,⁴ G. Jnawali,^{1,‡} H. Pfnür,⁴ C. Tegenkamp,⁴ P. Sutter,³
W. G. Schmidt,² and M. Horn-von Hoegen¹¹*Fakultät für Physik und Center for Nanointegration (CENIDE), Universität Duisburg-Essen, Lotharstrasse 1, 47057 Duisburg, Germany*²*Lehrstuhl für Theoretische Physik, Universität Paderborn, 33098 Paderborn, Germany*³*Center for Functional Nanomaterials, Brookhaven National Laboratory, Upton, New York 11973, USA*⁴*Institut für Festkörperphysik, Leibniz Universität Hannover, Appelstrasse 2, Hannover, Germany*

(Received 11 December 2014; revised manuscript received 1 May 2015; published xxxxx)

By combining scanning tunneling microscopy with density functional theory it is shown that the Bi(111) surface provides a well-defined incorporation site in the first bilayer that traps highly coordinating atoms such as transition metals (TMs) or noble metals. All deposited atoms assume exactly the same specific sevenfold coordinated subsurface interstitial site while the surface topography remains nearly unchanged. Notably, 3d TMs show a *barrier-free* incorporation. The observed surface modification by barrier-free subsorption helps to suppress aggregation in clusters. It allows a tuning of the electronic properties not only for the pure Bi(111) surface, but may also be observed for topological insulators formed by substrate-stabilized Bi bilayers.

DOI: [10.1103/PhysRevB.00.005400](https://doi.org/10.1103/PhysRevB.00.005400)

PACS number(s): 68.43.Fg, 68.37.Ef, 68.43.Bc, 73.20.-r

I. INTRODUCTION

Materials with spin-polarized two-dimensional (2D) surface states arising from the Rashba effect and topological insulators are of large potential interest for spintronic or dissipationless devices. Among the special properties of such systems are the suppression of backscattering, the existence of spin-polarized currents, and the topological protection of the surface state. Besides bismuth chalcogenides such as Bi₂Se₃ and Bi₂Te₃, also Bi bulk is a well-known model system for materials with strongly spin-split surface states [1–6]. Application of these novel material systems, however, requires the controlled tuning of properties such as band gap, carrier density, or doping level by electronic or morphological manipulation [7–11]. Often the electron transport in 2D surface electron systems is strongly influenced by individual scatterers, e.g., single atoms or molecules [7,8,12]. Unintentional defects such as step edges or impurities frequently show pronounced scattering patterns in scanning tunneling microscopy (STM) [7,13–19]. In contrast to these uncontrolled surface modifications, the deposition of single atoms at the surface, usually followed by thermally activated in-diffusion, allows for intentional doping of the near-surface region. Such controlled modification was recently reported for Bi₂Se₃ and Bi₂Te₃ compound films [18,20,21]. Depending on deposition temperature and subsequent annealing, Fe atoms occupy, however, various different metastable interstitial or substitutional sites [20].

In this work, we apply a similar approach to high-quality (111) bismuth films and demonstrate the incorporation of individual impurity atoms into highly specific, well-defined subsurface interstitial sites: Combining STM and density functional theory (DFT), we show that the first Bi bilayer traps transition metal (TM) or noble metal atoms in exactly

the same highly coordinated interstitial site. Moreover, 3d TMs such as Fe, Co, and Ni show a barrier-free incorporation. No thermal activation is required. Even at temperature below 10 K, the deposited atoms occupy always the same sevenfold coordinated subsurface site. The neighboring Bi atoms relax towards the interstitial impurity atom, but do not protrude and, thus, the surface remains structurally almost unchanged. This contrasts with typical adsorption, surface alloying, or surface reconstruction phenomena. In the following, we will refer to this special kind of surface modification as *subsorption*. It allows for the preparation of nominally undoped systems with metallic and even ferromagnetic electronic states, where backscattering is still suppressed by Rashba splitting. The barrier-free subsorption is not restricted to pure Bi(111) surfaces, but may also be found in the case of Bi(111) bilayer islands and substrate-stabilized Bi bilayers [19,22–26].

II. EXPERIMENTAL DETAILS

Ultrastable low-temperature scanning tunneling microscopy (LT-STM) was used to image and identify Friedel-like electronic scattering patterns as fingerprints for foreign atoms in a subsorption site. All experiments were performed under ultrahigh-vacuum (UHV) conditions. The preparation chamber had a base pressure below 2×10^{-10} mbar. The measurements were performed using a LT-STM in a bath cryostat at a pressure below the detection limit of 10^{-13} mbar and a base temperature of 5 K. Virtual Bi(111) substrates were grown on Si samples cut from an As-doped Si(111) wafer with a miscut below 0.1° and a resistivity of $0.004 \Omega \text{ cm}$ at room temperature. All samples were degassed in the load lock for 12 h at a temperature of 600°C prior to transfer into UHV. A short flash annealing cycle up to 1200°C was performed to remove the native oxide resulting in a clear (7×7) reconstruction on Si(111). Afterwards Bi was deposited by evaporation from a ceramic crucible heated by a tantalum filament. Bi(111) films were prepared by deposition of 20 nm of Bi at a sample temperature of 80 K, followed by an additional annealing step for 30 min at 200°C [27]. This preparation results in an atomically smooth surface with

*claudius.klein@uni-due.de

†uwe.gerstmann@uni-paderborn.de

‡Present address: Department of Physics and Astronomy, University of Pittsburgh, Pittsburgh 15260, USA.

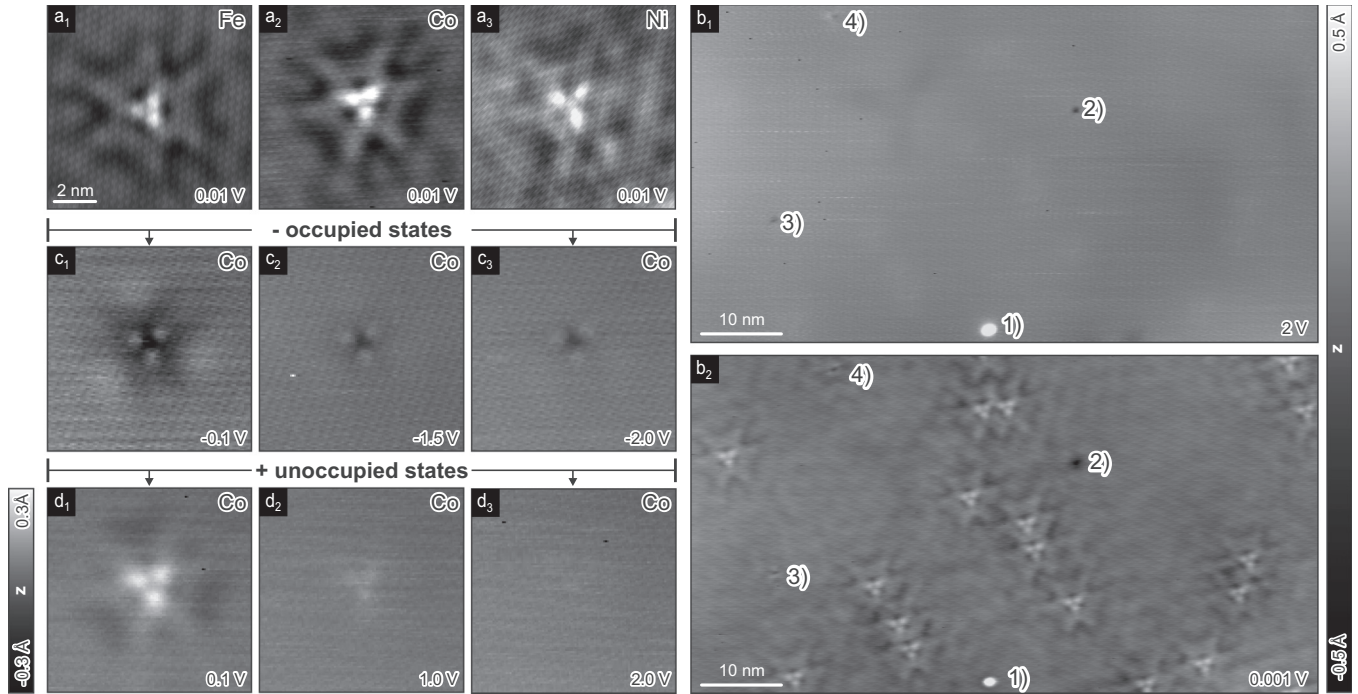


FIG. 1. (a₁–a₃) examples of various impurity atoms: Fe, Co, and Ni. (b₁) and (b₂) show a STM image of single Co impurities on a 20 nm Bi(111) film in constant current mode and identical z scale (-0.5 to 0.5 Å), taken under different conditions: (b₁) $I = 0.05$ nA, $U_{\text{Bias}} = 2$ V, and (b₂) $I = 0.05$ nA, $U_{\text{Bias}} = 1$ mV. The markers 1) to 4) indicate few other impurities or defects of unknown origin. (c₁–c₃) and (d₁–d₃): Series of a single Co impurity for various U_{Bias} ranging from -2 to $+2$ V. The z scale (-0.3 to 0.3 Å) is identical in all the images (a), (c), and (d).

89 terrace widths of more than 100 nm. The film quality was
 90 verified *in-situ* by low-energy electron diffraction (LEED) and
 91 STM. The low-temperature electron transport in such Bi films
 92 is dominated by a high density of surface-state electrons of
 93 about $10^{13}/\text{cm}^2$ and a negligible carrier concentration in the
 94 film bulk [28,29]. Submonolayer (ML) amounts of single-atom
 95 metal impurities were deposited onto the bare Bi films at 5 K
 96 into the STM without detaching the sample. Thereby we used a
 97 home-built microevaporator mounted on a transferable sample
 98 plate. During deposition the sample temperature increased
 99 by less than $\Delta T = 10$ K, due to radiation of the evaporator
 100 filament. The Bi(111) bilayer step height of 3.94 Å was used
 101 as calibration for the z piezo. Figures 1(a₁)–1(a₃) show STM
 102 micrographs in constant current mode after deposition of about
 103 0.005 ML of the transition metal impurities Fe, Co, and Ni at a
 104 base temperature of 5 K (1 ML corresponds to 1 atomic layer of
 105 the Bi(111) surface, i.e., $1 \text{ ML} = 5.6 \times 10^{14}$ atoms/cm²). Each
 106 impurity is surrounded by a threefold pattern of an apparent
 107 height modulation of $\Delta z = +0.3$ Å to -0.1 Å.

108 We choose the example of Co to investigate the nature and
 109 origin of the threefold patterns in more detail. Surprisingly, no
 110 signs of the deposited TM atoms are visible in Fig. 1(b₁),
 111 which shows an overview STM image obtained at a bias
 112 voltage of $U = +2.0$ V. Only a few unidentified impurities or
 113 defects (labeled 1–4 in Fig. 1) are present. They do not show
 114 any scattering pattern, but can still be identified at tunneling
 115 conditions close to the Fermi level $U_{\text{Bias}} \cong 0$ V [see Fig. 1(b₂)].
 116 At this bias voltage, additional extended patterns with threefold
 117 symmetry become apparent, which were not observed prior to
 118 Co deposition. All of these threefold patterns have the same
 119 orientation, shape, apparent vertical amplitude, and lateral size.

The density of these highly specific patterns scales with the Co
 120 deposition time, suggesting that the patterns coincide with the
 121 location of the Co atoms. Each pattern is thus indicative for
 122 the presence of a single Co atom located at the center of the
 123 pattern in the same geometrical site on or within the Bi film,
 124 interacting with (i.e., scattering) 2D electrons in the Bi(111)
 125 surface state.

126 Figures 1(c₁)–1(c₃) and 1(d₁)–1(d₃) show a single Co
 127 impurity for different bias voltages in higher resolution.
 128 Dominated by three light spots with trigonal symmetry, the
 129 pattern can be observed for positive and negative bias voltages,
 130 i.e., for occupied and empty states, close to the Fermi energy.
 131 The contrast and shape of the pattern, however, change
 132 significantly when varying the tunneling conditions in this
 133 regime. Some of the outer features in the threefold pattern even
 134 undergo a contrast inversion. The dispersion of the pattern,
 135 the weak amplitude at negative bias, and in particular the
 136 apparent absence of morphological features for higher bias
 137 voltages above 1 eV [see Fig. 1(d₃)] exclude a geometric
 138 height undulation as its origin. In contrast to Refs. [7,8], where
 139 morphological features such as Bi adatoms or clusters cause
 140 comparable scattering patterns, we do not observe any feature
 141 in the center of the Co-induced pattern. The pattern resembles,
 142 however, those in Bi₂Te₃(111) films where Fe atoms occupy
 143 substitutional Bi sites [20].
 144

145 III. COMPUTATIONAL METHOD

146 The experimental observations strongly evidence that even
 147 without thermal activation all Co atoms are incorporated into
 148 the Bi film at identical subsurface sites without any morpho-

logical modification at the surface. In order to rationalize this surprising experimental finding, DFT total-energy calculations were performed. The QUANTUM ESPRESSO package [30] was used, employing the gradient-corrected PBE functional [31] for the description of the electron exchange and correlation. Relativistic effects are taken into account on different levels of theory: While for structure relaxation a scalar-relativistic description is found to be sufficient, spin-orbit coupling affects the details of the electronic structure considerably [5]. Hence, spectroscopic properties such as magnetic moments require multicomponent relativistic calculations [32,33] with noncollinear spin polarization. The latter is visualized by arrows in Figs. 2(b) and 2(c) for the calculated subsorption configurations I and II, respectively.

The Bi(111) surface is modeled by periodic supercells, which contain between 6 and 22 Bi bilayers [34] separated by 20 Å vacuum. The atoms in the bottom bilayer are kept fixed at their ideal bulk positions. All other atoms are freely relaxed. Numerically converged subsorption geometries are obtained using a $6 \times 6 \times 1$ Brillouin zone sampling and require 6 Bi(111) bilayer slabs with a (4×4) translational symmetry. Hence, the Bi(111) surface structure contains 193 Bi atoms, including the impurity. The incorporation energy profiles are investigated by keeping the z coordinate of the adatom fixed. Its lateral position, as well as the Bi atoms within the three uppermost bilayers are freely relaxed. Migration barriers are calculated by explicitly determining the corresponding saddle points via the nudged elastic band (NEB) approach [35].

IV. RESULTS AND DISCUSSION

The resulting reaction paths are shown in Fig. 2(a). In principle, the adatoms could adsorb at the surface (i) singly

coordinated on top of a Bi atom of the first Bi layer or (ii) in two different threefold coordinated positions. However, for all investigated TM atoms a subsorbate position within the first Bi bilayer is the most stable configuration [labeled I in Fig. 2(a)]. Here, similar to the $\text{CoSi}_2/\text{Si}(111)$ interface [36], the TM atoms are sevenfold coordinated: Six bonds are formed to the ligands within the first Bi bilayer. A seventh Bi atom from the second bilayer binds to the TM atom.

Interestingly, for the $3d$ transition metals the subsorbate incorporation in the first Bi bilayer turns out to be barrier free; i.e., no thermal activation is required. Only Sc shows a very weak, metastable minimum 0.48 Å above the surface separated by a very shallow barrier $\Delta E < 0.01$ eV from the stable subsorbate configuration. The interstitial configuration I is by far (~ 1.1 eV) more stable than any substitutional incorporation, but energetically nearly degenerate with the fivefold coordinated interlayer position II [cf. Fig. 2(a)] as well as further intralayer positions deeper below the surface. However, migration into subsurface sites beyond configuration II is hindered by energy barriers of about 0.7 eV (Co) to 0.9 eV (Fe). The lateral mobility is restricted as well, but remains more probable: A lateral movement via configuration II and back into the top bilayer [cf. arrow in Fig. 2(a)] requires activation energies below 0.5 eV, and should thus occur prior to in-diffusion into the bulk.

The computational finding that the $3d$ TMs are captured at specific high-symmetry, sevenfold coordinated positions within the uppermost Bi bilayer is further corroborated by the comparison of the measured STM images with simulations based on the Tersoff-Hamann approach [37]: Only for the high-symmetry configuration I we obtain agreement with the measured STM data [cf. Fig. 1(d₁) and Fig. 2 showing Co as an example]. The three pronounced spots arise from p -like

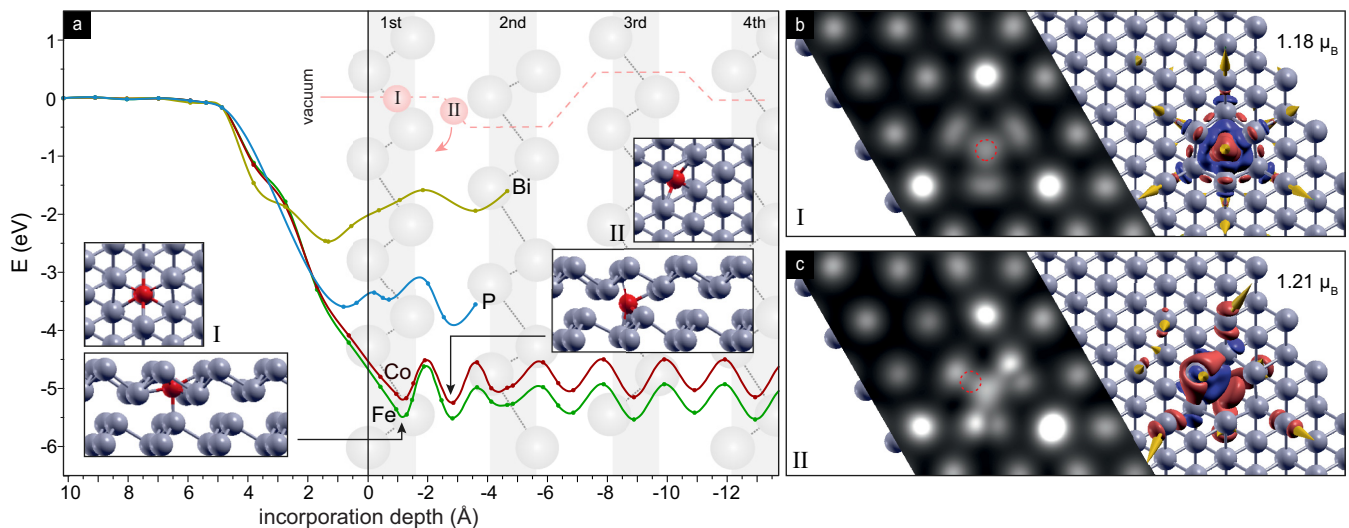


FIG. 2. (Color online) (a) Total energy for various adatom positions and different atomic species (Fe, Co, P, and Bi), the microscopic structures of the first (I) and second minimum (II), and the schematic migration path for a $3d$ TM atom (here Co) into the Bi bulk (arrow: relaxation in interlayer position as requirement for lateral motion). (b,c) Calculated STM image (constant current mode; $U = 10$ mV) for a single Co impurity in the highly symmetric sevenfold coordinated minimum I in the first bilayer and for the fivefold coordinated minimum II between two Bi bilayers. The red dashed circles indicate the position of the impurity Co atom. Co assumes a ferromagnetic configuration in both minima. The magnetization density induced by Co in minimum I and II (magnetic moments 1.18 and $1.21 \mu_B$, respectively) as well as the noncollinear spin orientation are indicated.

TABLE I. Calculated adsorption and incorporation energies (exothermic, in eV, relative to the respective free atom, metastable minima in brackets) calculated for various third, fourth, and fifth row element adatoms at or into the Bi(111) surface. If existing, energy barriers ΔE for the incorporation into the first Bi layer are also given.

	Sc	Ti	V	Cr	Mn	Fe	Co	Ni	Cu	Zn
Top	(3.53)	–	–	–	–	–	–	–	–	0.49
First BL	4.24	5.34	5.92	6.10	5.86	5.48	5.20	4.80	4.01	(0.26)
ΔE	<0.01	–	–	–	–	–	–	–	–	0.27
								Pd	Ag	
Top								(2.81)	(1.71)	
First BL								3.80	1.91	
ΔE								0.05	0.10	
	Bi	Pb						Pt	Au	
Top	2.60	2.61						(0.46)	(2.13)	
First BL	(1.58)	(1.75)						1.54	2.34	
ΔE	0.89	0.24						0.15	0.17	

215 orbitals at the next-nearest neighbor Bi surface atoms. The
 216 outer features of the experimental STM pattern cannot be
 217 reproduced within the 298 \AA^2 surface of the (4×4) supercells,
 218 indicating that these features are resulting from delocalized
 219 2D host states perturbed by the TM atom. Further information
 220 on the modification of the surface charge upon adsorption
 221 of TMs can be obtained from the calculated magnetization
 222 density shown in Fig. 2(b). For Co a magnetic moment of
 223 about $1.2 \mu_B$ is calculated for both configurations, I as well
 224 as II. But the asymmetric charge distribution around the
 225 fivefold coordinated position II [cf. Fig. 2(c)] is not compatible
 226 with experiment: All measured STM images show scattering
 227 patterns with trigonal symmetry, indicative for configuration
 228 I. The impurities have apparently no transient mobility into
 229 the bulk. The energy gained from surface bonding is lost in
 230 dissipative processes during adsorption and desorption, and
 231 the $3d$ TM atoms are trapped within the uppermost Bi bilayer.
 232 Thereby, the Fermi level is lifted by less than 10 meV with
 233 respect to the host states. It is their interstitial incorporation
 234 that allows the $3d$ TM impurity atoms to interact magnetically
 235 with the Rashba-split surface states (cf. Fig. 2) while only
 236 weakly perturbing the band structure.

237 In order to understand the special role of the $3d$ TMs,
 238 i.e., why they penetrate barrier-free, it is instructive to
 239 analyze the modification of their electronic configuration upon
 240 incorporation. The small shoulder in the energy profiles at
 241 about 3 \AA above the first Bi bilayer [see Fig. 2(a)] is related
 242 to the onset of an electronic reconfiguration: The $3d$ TM
 243 atoms change their $3d^n 4s^2$ electronic configuration due to
 244 the interaction with the host material; i.e., the $4s$ levels are
 245 energetically lifted and donate charge into the d orbitals, a
 246 phenomenon well known for $3d$ TM point defects in bulk
 247 semiconductors [38,39] which allows the formation of highly
 248 coordinated σ bonds to neighboring atoms [40]. In the case of
 249 Co ($[\text{Ar}]3d^7 4s^2$) approaching the Bi(111) film, for example,
 250 we find the occupation of the $4s$ states to be reduced to 0.64 and
 251 0.47 electrons, 3 \AA above and incorporated into the surface,
 252 respectively.

253 Looking at the process of incorporation in detail, the $3d$
 254 TM atom first relaxes into the uppermost Bi layer and forms
 255 a planar configuration with three Bi ligands. Concurrently, the

256 $3d$ electrons are polarized by the second layer Bi atoms and
 257 the impurity atom relaxes further without barrier towards the
 258 preferred, highly coordinated subsorbate position I within the
 259 Bi bilayer (see Fig. 2). The Bi lattice itself experiences only
 260 minor strain upon incorporation: The Bi-Bi bonds around the
 261 subsorbate change their length by amounts ranging from 2%
 262 (for Sc) up to at most 6% (for Cr). This is mainly related to
 263 a downwards relaxation of the second layer Bi atoms around
 264 the impurity. The topmost Bi atoms move laterally *towards* the
 265 impurity, but do essentially not vary their height; see inset I of
 266 Fig. 2. This agrees with the experimental observation that the
 267 topography of the surface remains unchanged.

268 $4d/5d$ TMs such as Pd and Pt also have partially filled
 269 d shells, but tend to form longer bonds with Bi. While their
 270 incorporation in the first Bi bilayer is still favorable, they have
 271 to overcome energy barriers ΔE of up to 0.2 eV (see Table I).
 272 This also holds for the noble metals Ag and Au. Atoms without
 273 partially filled d shell such as Zn, Bi, or Pb and even rather
 274 small atoms such as P and H cannot take advantage of the
 275 highly coordinated bonding position within the Bi bilayer.
 276 This position is either metastable or unstable for these atoms
 277 [cf. P and Bi in Fig. 2(a)] and they adsorb atop the surface.

278 That the barrier-free incorporation is actually a bond-length
 279 sensitive effect can also be seen by modifying the lateral
 280 lattice constant. This is of particular relevance for strained
 281 Bi(111) bilayer islands and substrate-stabilized Bi bilayers
 282 [22,23,19,24–26]. To obtain first estimates of how the atomic
 283 penetration will be influenced by strain, we perform additional
 284 total-energy calculations using single Bi(111) bilayers as a
 285 model systems. Thereby a barrier-free $3d$ TM incorporation
 286 into the bilayer is predicted, provided they are not too strongly
 287 strained. In case of Co deposition, for example, barrier-free
 288 incorporation occurs for bilayer strain between -5% and
 289 $+8\%$. For larger compression the lateral distance between
 290 neighboring Bi atoms and for more tensile strain above
 291 $+8\%$ the distance between the two Bi layers becomes too
 292 small. Therefore, we expect also systems that contain single,
 293 substrate-stabilized Bi(111) bilayers to be susceptible to the
 294 barrier-free incorporation, provided the lattice constant of the
 295 substrate is close to that of the Bi(111) surface. Hexagonal
 296 BN (-2%) or Bi_2Te_3 (-5%), e.g., fulfill this requirement. For

297 Bi_2Se_3 , however, causing 11% compressive strain, thermal
 298 activation is required for a subsurface in-diffusion into the Bi
 299 bilayer.

V. SUMMARY

300
 301 In this work, it has been demonstrated that the Bi(111)
 302 surface provides a specific incorporation site within the first
 303 bilayer, which is attractive for highly coordinated transition
 304 and noble metal atoms. They are found to penetrate the surface
 305 in a well defined way, thereby causing no morphological
 306 changes at the surface. In contrast to thermally activated
 307 in-diffusion recently found for Bi_2Se_3 and Bi_2Te_3 compound
 308 films [18,20,21], the incorporation of $3d$ TM into Bi(111)
 309 films occurs barrier-free. No annealing step is required
 310 reducing the probability for lateral migration and unwanted
 311 aggregation of the TM atoms in clusters to a minimum.
 312 Hence, high doping concentration become possible, and each
 313 atom assumes a well-defined sevenfold coordinated interstitial

position, providing a metallic near-surface state by only 314
 weakly perturbing the band structure. The observed surface 315
 modification by barrier-free subsorption does not only allow 316
 for tuning the electronic properties of the Bi surfaces itself, 317
 but may also be applicable to topological insulators formed by 318
 substrate-stabilized Bi bilayers, provided the lattice constant of 319
 the substrate resembles within a few percent that of the Bi(111) 320
 surface; otherwise in-diffusion requires thermal activation. 321

ACKNOWLEDGMENTS

We acknowledge financial support by the DFG through 323
 SFB 616, SPP 1601, and Pf238/31 as well as grants of 324
 high-performance computer time from the HLRS Stuttgart 325
 and the Paderborn PC². Research was carried out in part at the 326
 Center for Functional Nanomaterials, Brookhaven National 327
 Laboratory, which is supported by the U.S. Department of 328
 Energy, Office of Basic Energy Sciences, under Contract No. 329
 DE-AC02-98CH10886. 330

-
- [1] C. R. Ast, J. Henk, A. Ernst, L. Moreschini, M. C. Falub, D. Pacile, P. Bruno, K. Kern, and M. Grioni, *Phys. Rev. Lett.* **98**, 186807 (2007).
- [2] Ph. Hofmann, *Prog. Surf. Sci.* **81**, 191 (2006).
- [3] T. Hirahara, T. Nagao, I. Matsuda, G. Bihlmayer, E. V. Chulkov, Yu. M. Koroteev, P. M. Echenique, M. Saito, and S. Hasegawa, *Phys. Rev. Lett.* **97**, 146803 (2006).
- [4] E. I. Rashba, *Sov. Phys. Solid State* **2**, 1109 (1960).
- [5] Yu. M. Koroteev, G. Bihlmayer, J. E. Gayone, E. V. Chulkov, S. Blügel, P. M. Echenique, and Ph. Hofmann, *Phys. Rev. Lett.* **93**, 046403 (2004).
- [6] T. Hirahara, K. Miyamoto, I. Matsuda, T. Kadono, A. Kimura, T. Nagao, G. Bihlmayer, E. V. Chulkov, S. Qiao, K. Shimada, H. Namatame, M. Taniguchi, and S. Hasegawa, *Phys. Rev. B* **76**, 153305 (2007).
- [7] M. C. Cottin, C. A. Bobisch, J. Schaffert, G. Jnawali, A. Sonntag, G. Bihlmayer, and R. Möller, *Appl. Phys. Lett.* **98**, 022108 (2011).
- [8] G. Jnawali, C. Klein, Th. Wagner, H. Hattab, P. Zahl, D. P. Acharya, P. Sutter, A. Lorke, and M. Horn-von Hoegen, *Phys. Rev. Lett.* **108**, 266804 (2012).
- [9] Z. Wang, T. Lin, P. Wei, X. Liu, R. Dumas, K. Liu, and J. Shi, *Appl. Phys. Lett.* **97**, 042112 (2010).
- [10] D. Hsieh, Y. Xia, L. Wray, D. Qian, A. Pal, J. H. Dil, J. Osterwalder, F. Meier, G. Bihlmayer, C. L. Kane, Y. S. Hor, R. J. Cava, and M. Z. Hasan, *Science* **323**, 919 (2009).
- [11] T. Hirahara, N. Fukui, T. Shirasawa, M. Yamada, M. Aitani, H. Miyazaki, M. Matsunami, S. Kimura, T. Takahashi, S. Hasegawa, and K. Kobayashi, *Phys. Rev. Lett.* **109**, 227401 (2012).
- [12] D. Lükermann, S. Sologub, H. Pfnür, C. Klein, M. Horn-von Hoegen, and C. Tegenkamp, *Phys. Rev. B* **86**, 195432 (2012).
- [13] Z. Alpichshev, R. R. Biswas, A. V. Balatsky, J. G. Analytis, J.-H. Chu, I. R. Fisher, and A. Kapitulnik, *Phys. Rev. Lett.* **108**, 206402 (2012).
- [14] G. Wang, X.-G. Zhu, Y.-Y. Sun, Y.-Y. Li, T. Zhang, J. Wen, X. Chen, K. He, L.-L. Wang, X.-C. Ma, J.-F. Jia, S. B. Zhang, and Q.-K. Xue, *Adv. Mater.* **23**, 2929 (2011).
- [15] C. Mann, D. West, I. Miotowski, Y. P. Cheng, S. Zhang, and C.-K. Shih, *Nat. Commun.* **4**, 2277 (2013).
- [16] T. Zhang, P. Cheng, X. Chen, J.-F. Jia, X. Ma, K. He, L. Wang, H. Zhang, X. Dai, Z. Fang, X. Xie, and Q.-K. Xue, *Phys. Rev. Lett.* **103**, 266803 (2009).
- [17] J. Seo, P. Roushan, H. Beidenkopf, Y.-S. Hor, R.-J. Cava, and A. Yazdani, *Nature* **466**, 343 (2010).
- [18] T. Schlenk, M. Bianchi, M. Koleini, A. Eich, O. Pietzsch, T. O. Wehling, T. Frauenheim, A. Balatsky, J.-L. Mi, B. B. Iversen, J. Wiebe, A. A. Khajetoorians, Ph. Hofmann, and R. Wiesendanger, *Phys. Rev. Lett.* **110**, 126804 (2013).
- [19] M. Cottin, C. A. Bobisch, J. Schaffert, G. Jnawali, G. Bihlmayer, and R. Möller, *Nano Lett.* **13**, 2717 (2013).
- [20] D. West, Y. Y. Sun, S. B. Zhang, T. Zhang, X. Ma, P. Cheng, Y. Y. Zhang, X. Chen, J. F. Jia, and Q. K. Xue, *Phys. Rev. B* **85**, 081305(R) (2012).
- [21] C. L. Song, Y. P. Jiang, Y. L. Wang, Z. Li, L. Wang, K. He, X. Chen, X. C. Ma, and Q. K. Xue, *Phys. Rev. B* **86**, 045441 (2012).
- [22] T. Hirahara, G. Bihlmayer, Y. Sakamoto, M. Yamada, H. Miyazaki, S. Kimura, S. Blügel, and S. Hasegawa, *Phys. Rev. Lett.* **107**, 166801 (2011).
- [23] M. Chen, J.-P. Peng, H.-M. Zhang, L.-L. Wang, K. He, X.-C. Ma, and Q.-K. Xue, *Appl. Phys. Lett.* **101**, 081603 (2012).
- [24] S. H. Kim, K.-H. Jin, J. Park, J. S. Kim, S.-H. Jhi, T.-H. Kim, and H. W. Yeom, *Phys. Rev. B* **89**, 155436 (2014).
- [25] A. Eich, M. Michiardi, G. Bihlmayer, X.-G. Zhu, J.-L. Mi, B. B. Iversen, R. Wiesendanger, Ph. Hofmann, A. A. Khajetoorians, and J. Wiebe, *Phys. Rev. B* **90**, 155414 (2014).
- [26] I. K. Drozdov, A. Alexandradinata, S. Jeon, S. Nadj-Perge, H. Ji, R. J. Cava, B. A. Bernevig, and A. Yazdani, *Nat. Phys.* **10**, 664 (2014).
- [27] T. Payer, C. Klein, M. Acet, V. Ney, M. Kammler, F.-J. Meyer zu Heringdorf, and M. Horn-von Hoegen, *Thin Solid Films* **520**, 6905 (2012).
- [28] G. Jnawali, Th. Wagner, H. Hattab, R. Möller, A. Lorke, and M. Horn-von Hoegen, *e-J. Surf. Sci. Nanotechnol.* **8**, 27 (2010).

- [29] T. Hirahara, I. Matsuda, S. Yamazaki, N. Miyata, S. Hasegawa, and T. Nagao, *Appl. Phys. Lett.* **91**, 202106 (2007).
- [30] P. Giannozzi *et al.*, *J. Phys.: Condens. Matter* **21**, 395502 (2009); <http://www.quantum-espresso.org>.
- [31] J. P. Perdew, K. Burke, and M. Ernzerhof, *Phys. Rev. Lett.* **77**, 3865 (1996).
- [32] A. DalCorso, *Phys. Rev. B* **82**, 075116 (2010).
- [33] U. Gerstmann, N. J. Vollmers, A. Lücke, M. Babilon, and W. G. Schmidt, *Phys. Rev. B* **89**, 165431 (2014).
- [34] Y. M. Koroteev, G. Bihlmayer, E. V. Chulkov, and S. Blügel, *Phys. Rev. B* **77**, 045428 (2008).
- [35] G. Henkelmann and H. Jónsson, *J. Chem. Phys.* **113**, 9978 (2000).
- [36] M. F. Chisholm, S. J. Pennycook, R. Jevasinski, and S. Mantl, *Appl. Phys. Lett.* **64**, 2409 (1994).
- [37] J. Tersoff and D. Hamann, *Phys. Rev. B* **31**, 805 (1985).
- [38] F. Beeler, O. K. Andersen, and M. Scheffler, *Phys. Rev. Lett.* **55**, 1498 (1985).
- [39] U. Gerstmann, A. T. Blumenau, and H. Overhof, *Phys. Rev. B* **63**, 075204 (2001).
- [40] A. Abragam and B. Bleaney, *Electron Paramagnetic Resonance of Transition Ions* (Dover Publications, New York, 1989).